Cell and Tissue Research (2018) 374:317–327
https://doi.org/10.1007/s00441-018-2869-z

REGULAR ARTICLE

Ultrastructural changes in endometrial desmosomes of desmoglein 2 mutant mice

Volker U. Buck[1] · Matthias Hodecker[1] · Sabine Eisner[1] · Rudolf E. Leube[1] · Claudia A. Krusche[1] · Irmgard Classen-Linke[1]

Received: 22 December 2017 / Accepted: 25 May 2018 / Published online: 25 June 2018
© Springer-Verlag GmbH Germany, part of Springer Nature 2018

Abstract

The intercellular binding of desmosomal junctions is mediated by cadherins of the desmoglein (Dsg) and desmocollin (Dsc) type. Dsg2 mutant mice with deletion of a substantial segment of the extracellular EC1-EC2 domain, which is believed to participate in homo- and heterophilic desmosomal cadherin interactions, develop cardiac fibrosis and ventricular dilation. Widening of the intercellular cleft and complete intercalated disc ruptures can be observed in the hearts of these mice. Since a reduced litter size of homozygous Dsg2 mutant mice was noted and a functional correlation between desmosomes and embryo implantation has been deduced from animal studies, we looked for an alteration of desmosomes in uterine endometrial epithelium. Shape and number of desmosomes as well as the expression of Dsg2 and the desmosomal plaque protein desmoplakin (Dsp) were investigated by electron microscopy and immunohistochemistry in 12 oestrous-dated mice (7 wild type and 5 homozygous Dsg2 mutant mice) at the age of 9–17 weeks. The immunohistochemical detection of Dsg2 was diminished in the mutants and the number of desmosomes was significantly reduced as revealed by electron microscopy. In addition, the intercellular desmosomal space measured in electron micrographs was considerably widened in the Dsg2 mutants. The increased intercellular spacing can be explained by the partial deletion of the extracellular EC1–EC2 domain of Dsg2. Whether these changes explain the reduced number of offspring of homozygous Dsg2 mutant mice remains to be further investigated.

Keywords Dsg2 mutant mice · ARVC · Endometrial uterine lining · Widened intercellular desmosomal space · Morphometric ultrastructural analysis

Introduction

The uterine luminal and glandular endometrial epithelium consists of a single layer of polarised columnar epithelial cells comparable to the mucosal epithelium of the intestine, stomach, gall bladder and oviduct. These typical polarised epithelia contain characteristic tripartite junctional complexes at apical cell–cell contact sites consisting of a zonula occludens at the top, a zonula adhaerens adjacent to it and multiple desmosomes situated below it (Farquhar and Palade 1963).

Desmosomes are prominent cell–cell contact structures in epithelia (Broussard et al. 2015; Garrod and Chidgey 2008; Holthofer et al. 2007; Kowalczyk and Green 2013; Thomason et al. 2010). They act as plasma membrane attachment sites for the keratin intermediate filament cytoskeleton and are responsible for cellular adhesion and tissue integrity. Desmosomal adhesion is mediated by desmosome-specific cadherins. These calcium-dependent adhesion molecules are membrane-spanning constituents of desmosomes. They exist in seven different isoforms in humans, i.e., desmogleins (Dsg) 1–4 and desmocollins (Dsc) 1–3 (Garrod and Chidgey 2008). Dsg2 and Dsc2 are the most abundant isoforms in desmosomes of absorptive and glandular simple epithelia including endometrial epithelium.

The Dsg2 gene was first identified by Koch et al. (1990, 1991). The mRNA has been cloned and the complete amino acid sequence determined by Schafer et al. (1994). Subsequently, Dsg2 was detected by various antibodies in different species, including human (Schafer et al. 1996).

Most studies on the structure of desmosomes have been performed either on stratified epithelium, i.e., keratinocytes, or on cardiomyocytes (Al-Amoudi et al. 2007; Al-Amoudi

✉ Irmgard Classen-Linke
iclassen-linke@ukaachen.de

[1] Institute of Molecular and Cellular Anatomy, RWTH Aachen University, Wendlingweg 2, 52074 Aachen, Germany

and Frangakis 2008). Fewer data are available on simple epithelia. A study by Schlegel et al. (2010) indicated that Dsg2-mediated adhesion affects tight junction integrity in intestinal epithelia and is required to maintain intestinal epithelial barrier properties. Loss of Dsg2 may be involved in cancer and contributes to the pathogenesis of Crohn's disease (Spindler et al. 2015). In addition to its importance for intercellular cohesion, Dsg2 may also be involved in important cellular functions such as proliferation (Kamekura et al. 2014), apoptosis and early development (Nava et al. 2007). Dsg2 knock-outs die during the early implantation phase (Eshkind et al. 2002).

The extracellular part of Dsg2 consists of the four calcium-binding domains EC1–EC4. Recently, a Dsg2 mutant mouse ($Dsg2^{mt}$) was generated lacking major parts of the extracellular EC1–EC2 domains (Holthofer 2007; Holthofer et al. 2007; Krusche et al. 2011).

These mutants develop a pathological cardiac phenotype with dilated atria and ventricles and exhibit cardiac fibrosis. Investigations by electron microscopy revealed a loss of desmosomes in the intercalated discs of mutant hearts and, in particular, widening of the intercellular space as well as dissociation of intercalated discs close to lesions (Kant et al. 2012).

Since a reduced litter size was noted in Dsg2 mutant mice (Krusche et al. 2011) and a functional correlation between desmosomes and embryo implantation has been deduced from animal studies (Illingworth et al. 2000; Preston et al. 2004; Preston et al. 2006) and from our own research on human trophoblast-endometrial interaction in cell culture (Buck et al. 2015), we looked for an alteration of desmosomes in uterine endometrial epithelium.

Although no obvious pathological changes besides the cardiac phenotype were observed in tissues containing Dsg2 such as intestine, liver and endometrium, we used electron microscopy and immunohistochemistry to investigate whether Dsg2 mutation affects the structure and function of desmosomal adhesion in the endometrial epithelium, which might in part explain the reduced number of offspring of the mutant mice.

Materials and methods

Animals

The Dsg2 mutant mouse ($Dsg2^{mt}$) lacks exons 4–6 of the Dsg2 gene (Holthofer et al. 2007; Krusche et al. 2011). These exons code for major parts of the extracellular EC1–EC2 domains and their deletion leads to loss of amino acids 78 (isoleucine) to 234 (arginine) of the desmoglein-2 precursor (*Mus musculus*), reference sequence NP_031909.2. This corresponds to the nucleotide sequence 441–914; NCBI reference sequence NM_007883.3.

Mice were housed in the animal facility of the RWTH University Hospital. The animals were supplied with standard rodent lab diet (Ssniff, Soest, Germany) and were given ad libitum access to food and water. In total, 12 adult females (7 wild type and 5 homozygous mutant animals) aged 9–17 weeks were used in this study. Wild type controls and homozygous mutant littermates (Table 1) were obtained by mating of heterozygous mutant mice. To exclude possible cyclic changes of desmosomal adhesion in the endometrial epithelium, all animals were subjected to oestrous cycle stage monitoring prior to autopsy.

Oestrous cycle stage monitoring

Oestrous cycle stage was determined by cytological examination of vaginal lavage material according to Rugh (1968) and Byers et al. (2012). One hundred microliters of 0.9% sodium chloride solution was applied to the vagina with a buttoned cannula and aspirated again. Aspirates were transferred to Super-Frost® plus glass slides (Thermo Fisher Scientific, Bonn, Germany), air-dried for 30 min at room temperature (RT) and fixed with methanol for 10 min (RT). Slides were then stained with Giemsa solution (1:50 (*v*/*v*) in H_2O) (Merck, Darmstadt, Germany) for 30 min (RT), rinsed in PBS and washed in deionised water. The slides were air-dried again for 30 min (RT) and mounted with DePeX (Serva, Heidelberg, Germany). Vaginal cytology was assessed 3 days and 24 h prior to autopsy. Oestrous cycle monitoring was performed once again on the day of autopsy and animals were sacrificed after evaluation of stained lavage material by light microscopy. Only animals with cytological features typical of the oestrous phase were included in the study.

Tissue collection

After monitoring of the oestrous cycle stage, animals were killed by cervical dislocation. One uterine horn was directly dissected in fixative (4% formaldehyde/1% glutaraldehyde) (McDowell and Trump 1976) and further processed for examination by electron microscopy. The other uterine horn was transferred to a cryogenic vial (Nalgene Nunc, Rochester, NY, USA) filled with Sakura Tissue-Tek® O.C.T. ™ Compound (Finetek, Alphen aan de Rijn, Netherlands), shock frozen in liquid nitrogen and stored at − 40 °C for further processing.

Immunofluorescence microscopy

Immunofluorescence staining was performed on 10-μm-thick cryostat sections from shock-frozen specimens mounted on Super-Frost® plus glass slides (Thermo Fisher Scientific,

Table 1 List of animals; ++,**, ## are siblings

Animal number	Dsg2-genotype	Age (weeks)	Ultrastructure	Immunohistochemistry
3826	wt/wt	14	+	–
3835	wt/wt	11	+	+
3896+	mt/mt	9	+	+
3898+	mt/mt	9	+	+
4009*	mt/mt	9	+	+
4017*	wt/wt	9	+	+
4025	wt/wt	10	+	+
4178	mt/mt	17	+	+
4182#	mt/mt	16	+	+
4186#	wt/wt	16	+	+
3851	wt/wt	11	–	+
4172	wt/wt	17	–	+

Bonn, Germany). Sections were fixed in acetone for 10 min at 4 °C, air-dried and stored at − 20 °C. Slides were rehydrated in PBS for 10 min and blocked for 20 min with 5% goat and/or donkey serum. Polyclonal rabbit antibody against the extracellular anchor domain and fourth extracellular domain (EC4) of Dsg2 (Holthofer et al. 2007; Schlegel et al. 2010) was diluted 1:1000. The polyclonal guinea pig antibody against desmoplakin 1/2 (DP 495, Progen Biotechnik, Heidelberg, Germany) was diluted 1:500. Antibodies were diluted with PBS supplemented with 1.5% bovine serum albumin. After incubation overnight at 4 °C with primary antibodies, slides were rinsed in PBS three times and then incubated for 1 h in the dark at room temperature with secondary antibodies (Cy3 donkey-anti-rabbit, Jackson, West Grove, USA; alexa 488 goat-anti-guinea pig, Invitrogen, Eugene, USA). For immunofluorescent double labelling, both primary antibodies were applied together. Similarly, both secondary antibodies were mixed in the next incubation step. Slides were counterstained with 40,6-diamidino-2-phenylindole, dihydrochloride (DAPI 1 μg/ml, Sigma, Hamburg, Germany) for 30 min at room temperature. Slides were then rinsed again three times in PBS and washed in deionised water. Sections were mounted with Kaiser's glycerol gelatin (Merck, Darmstadt, Germany) and stored at 4 °C for microscopic assessment. The specific primary antibodies were omitted for the controls. No specific staining of these negative controls was observed.

Fluorescence microscopy analysis

Fluorescent sections were assessed and scanned with a confocal laser scanning microscope (LSM 710 Duo, Zeiss, Jena, Germany) and evaluated using the ZEN 2009 software (Zeiss, Jena, Germany). Processing of exported z-stack slices for 3D animation was performed using the image-processing program FIJI based on ImageJ. All parameters concerning the confocal laser scanning adjustments, laser strength and the image processing were identical for all recordings.

Electron microscopy

Uteri of 8–16.5-week-old mice were studied by electron microscopy. The mice were cycle-monitored and the tissue was obtained at the oestrous stage. After cervical dislocation, uteri were excised and dissected in fixative (4% formaldehyde/1% glutaraldehyde; pH 7.4) (McDowell and Trump 1976). The samples were then minced into 1–2 mm^3 pieces, incubated for 2 h in fixative and for 1 h in 1% OsO4 in 0.2 M phosphate buffer (pH 7.3).The tissue was then treated with 0.5% uranyl acetate in 0.05 M sodium maleate buffer (pH 5.2) for 2 h in the dark. The tissue was dehydrated and embedded in araldite using acetone as intermedium. Polymerisation was carried out at 60 °C for 48 h. Semithin sections of 0.35 μm were obtained using glass knives and stained with toluidine blue. Ultrathin sections of 50 nm were then prepared with an ultramicrotome (Reichert Ultracut S, Leica, Wetzlar, Germany) using diamond knives. To enhance contrast, the sections on copper grids were first treated with 3% uranyl acetate for 5 min and then with lead citrate solution (according to Reynolds 1963) for 4 min. Images were taken on an EM 10 (Zeiss) with a digital camera (Olympus, Münster, Germany) using the iTEM software (Olympus).

Analysis of desmosomes on ultrathin sections

The luminal epithelium of the mouse endometrium was analysed at a magnification of 63,000. Only epithelial cells that were cut in a rectangular section with a distinct

nucleus and a clear apical/basal orientation were evaluated. No directly adjacent cells were evaluated. The number of desmosomes per cell was counted on the entire lateral plasma membrane surrounding the epithelial cell from the apical to the basal pole. In addition, the width and length of the two outer dense plaques (ODP) and the width of the intercellular space were measured. The desmosomes were analysed with two different methods in each specimen:

1. Linear measurement with the analysis software of Image-Pro Plus 5.0
2. Grey scale analysis with the line profile analysis tool of Image-Pro Plus 5.0

To minimise any bias, the grey scale analysis was performed by the same researcher (MH) blinded for the specimen.

Statistics

Statistical analyses were performed using GraphPad Prism, version 6 for Windows (GraphPad Software Inc., San Diego, USA).

The mean, the standard error of the mean (SEM) and the standard deviation (SD) were determined. The unpaired two-tailed *T* tests with Welch's correction were performed for statistical analysis. *P* values < 0.05 were considered to be significantly different.

Results

Macroscopic appearance of wild type and mutant uteri

The mutation of the DSG2 gene leads to a macroscopically visible cardiac phenotype which is characterised by dilation of atria and ventricles compared to $Dsg2^{wt/wt}$ animals (Fig. 1a, c). Moreover, fibrotic lesions can be discerned in mutant animals (Fig. 1c). In contrast, $Dsg2^{mt/mt}$ uteri of the same oestrous cycle stage did not reveal any obvious changes in size or diameter nor in gross morphology in comparison to $Dsg2^{wt/wt}$ uteri (Fig. 1b, d).

Immunofluorescence analysis of desmosomal proteins

An immunofluorescence study was performed on cross-sections of shock-frozen uteri from $Dsg2^{wt/wt}$ and $Dsg2^{mt/mt}$ animals to analyse the effect of mutant Dsg2 on the expression and localisation of desmosomes in this simple epithelium. Both luminal epithelial cells (Fig. 2) and epithelial cells of the deep peripheral crypts (Fig. 3) were assessed by double labelling with antibodies against the desmosomal plaque protein desmoplakin 1/2 (Dsp) and the desmosomal cadherin Dsg2. In luminal and glandular cross-sections of the mutant uterine endometrium, the Dsg2 fluorescence signal was strongly diminished compared to the Dsp staining intensity (Figs. 2 and 3). However, also the expression of Dsp was reduced in the mutant mice compared to the wild type indicating a decreased number of desmosomes.

Ultrastructural morphology of desmosomes

Images of desmosomes were taken in wild type and mutant mice at the same magnification of 63,000. Figures 4 and 5 show typical desmosomes of the wild type and mutant mouse uteri. Desmosomes are depicted near the apical surface (Fig. 4a, c) and more distantly at the lateral plasma membranes (Fig. 4b, d).

The broader intercellular space in the mutant desmosome is readily apparent in Fig. 5. The intercellular space in the desmosomes of the mutants (Fig. 5d) is light and without the dense material known as desmogloea. In the wild type, the intercellular space is filled with this dense material, although a midline cannot be discerned.

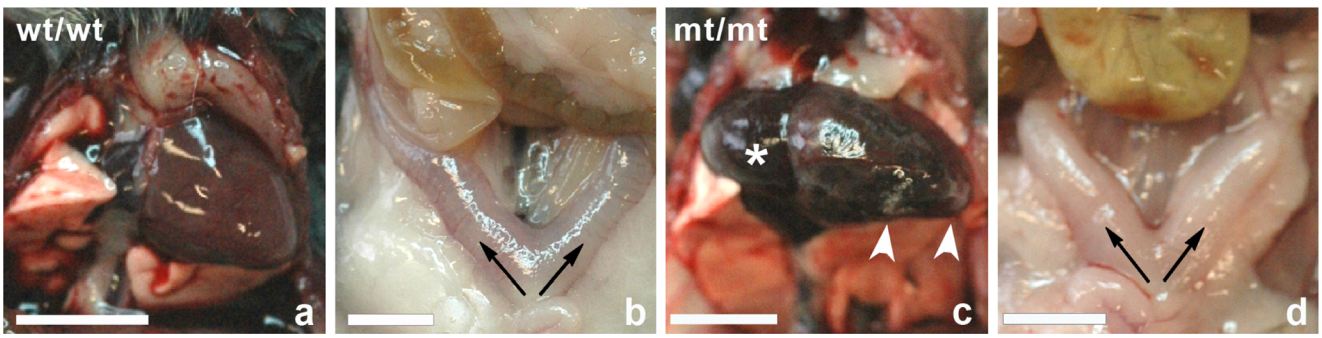

Fig. 1 Situs of a wild type mouse (wt/wt; **a**, **b**) in comparison to a mutant mouse (mt/mt; **c**, **d**). Dilation (asterisk) and fibrotic foci (arrowheads) can be seen in the mutant heart (**c**). The uterine horns (arrows) of the wild type (**b**) and the mutant mouse (**d**) do not differ in gross morphology. Scale bars 5 mm

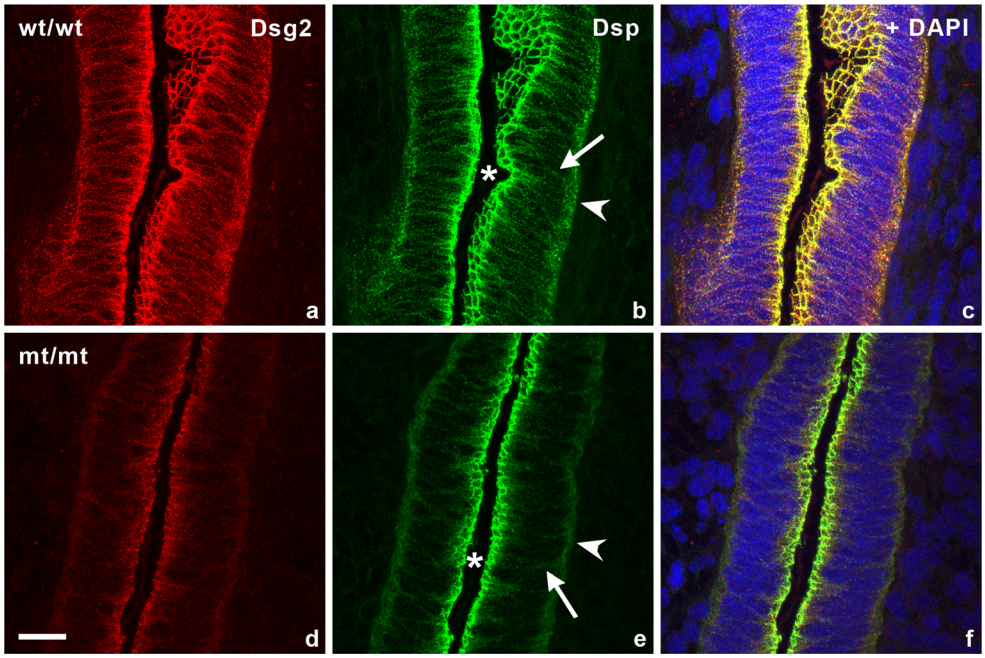

Fig. 2 Immunofluorescence staining of luminal endometrial epithelial cells from wild type (wt/wt; **a**–**c**) and homozygous Dsg2 mutant animals (mt/mt; **d**–**f**). Uteri were dissected during the oestrous stage. Double-label staining was performed against Dsg2 and the desmosomal plaque protein desmoplakin (Dsp) and combined with nuclear staining (DAPI). In both instances, the desmosomal proteins co-localised (**c**, **f**) and the highest concentration of desmosomal dots was found close to the lumen (asterisks) in the apical-most regions of the lateral plasma membranes. Furthermore, the desmosomal dots were equally distributed along the remaining lateral plasma membranes and also found close to the basal margin of the epithelial cells in the wild type (arrowhead in **b**). In contrast, luminal epithelial cells of mt/mt animals showed a decreased number of lateral desmosomal dots in the lower regions of the lateral plasma membranes (arrow in **e**) indicating a reduced number of desmosomes. Overall, the expression level of Dsg2 was reduced in homozygous mutants compared to the wild type (compare **a** and **d**). Scale bar 20 μm

Ultrastructural analysis of desmosomes

Desmosomes were counted per cell and their shape was measured according to certain assumptions as described in the "Material and methods" section and illustrated in Figs. 6 and 7. In total, 276 wild type and 319 mutant endometrial epithelial cells were evaluated. Desmosomes (895) were counted (wild type 500; mutant 395). The

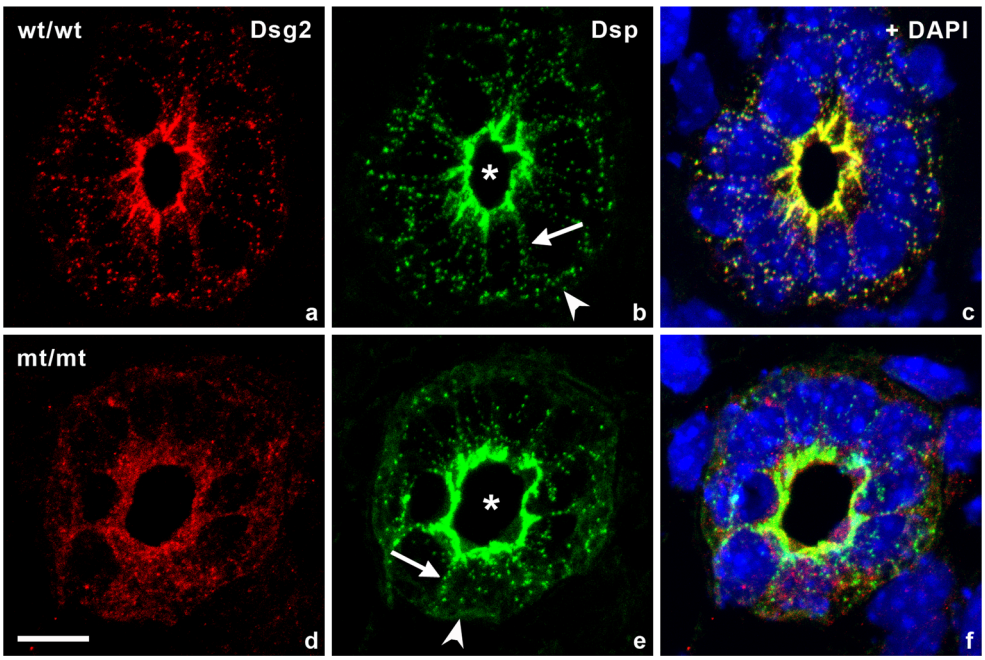

Fig. 3 Cross-sections through glandular endometrial epithelial cells from wild type (wt/wt; **a**–**c**) and homozygous mutant animals (mt/mt; **d**–**f**). Uteri were dissected during the oestrous stage. Immunofluorescence microscopy was performed using antibodies against Dsg2 and the desmosomal plaque protein desmoplakin (Dsp) combined with nuclear staining (DAPI). Dsg2 expression was strongly diminished in mutant mice (**d**). Asterisks: lumen; arrows: lateral plasma membranes; arrowheads: basal margins of epithelial cells. Scale bar 10 μm

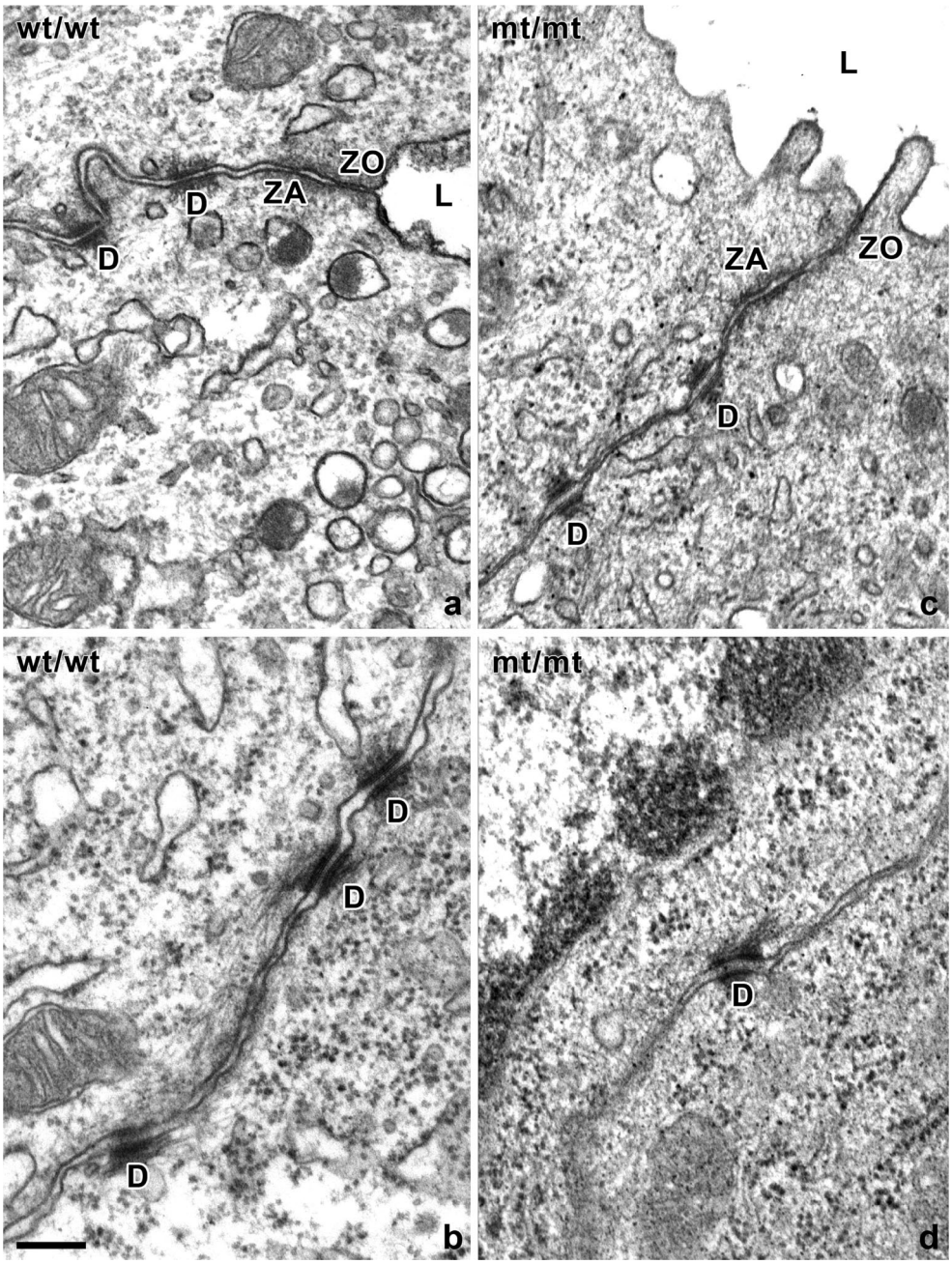

Fig. 4 Comparison of typical desmosomes in the endometrial epithelium of wild type (wt/wt; **a**, **b**) and mutant mice (mt/mt; **c**, **d**). In **a** and **c**, the tripartite junctional complex consisting of zonula occludens (ZO), zonula adhaerens (ZA) and desmosomes (D) can be seen close to the lumen (L). In **b** and **d**, lower regions of the lateral plasma membranes are shown. Scale bar 200 nm

mean value ± SEM for the number of desmosomes per cell was 1.81 ± 0.09 in the wild type and 1.24±0.07 in the mutant. The means were significantly different: $p < 0.0001$.

Linear measurement with the analysis software of Image-Pro Plus 5.0

Of all the counted desmosomes (wild type 180; mutant 209), it was possible to analyse 389 by linear measurement with the analysis software of Image-Pro Plus 5.0. The mean ± SEM of the intercellular space for the wild type was 14.9 ± 0.32 nm and for the mutant 19.1 ± 0.35 nm (Fig. 7). The means of the measured width of the intercellular space were significantly different: $p < 0.0001$.

In contrast, the means of the measured width and length of the two outer dense plaques did not change significantly between wild type and mutant.

The mean ± SEM of the width of the ODP was 17.10 ± 0.19 nm for the wild type and 16.76 ± 0.17 nm, $p = 0.20$, for the mutant. The mean ± SEM of the length of the ODP was

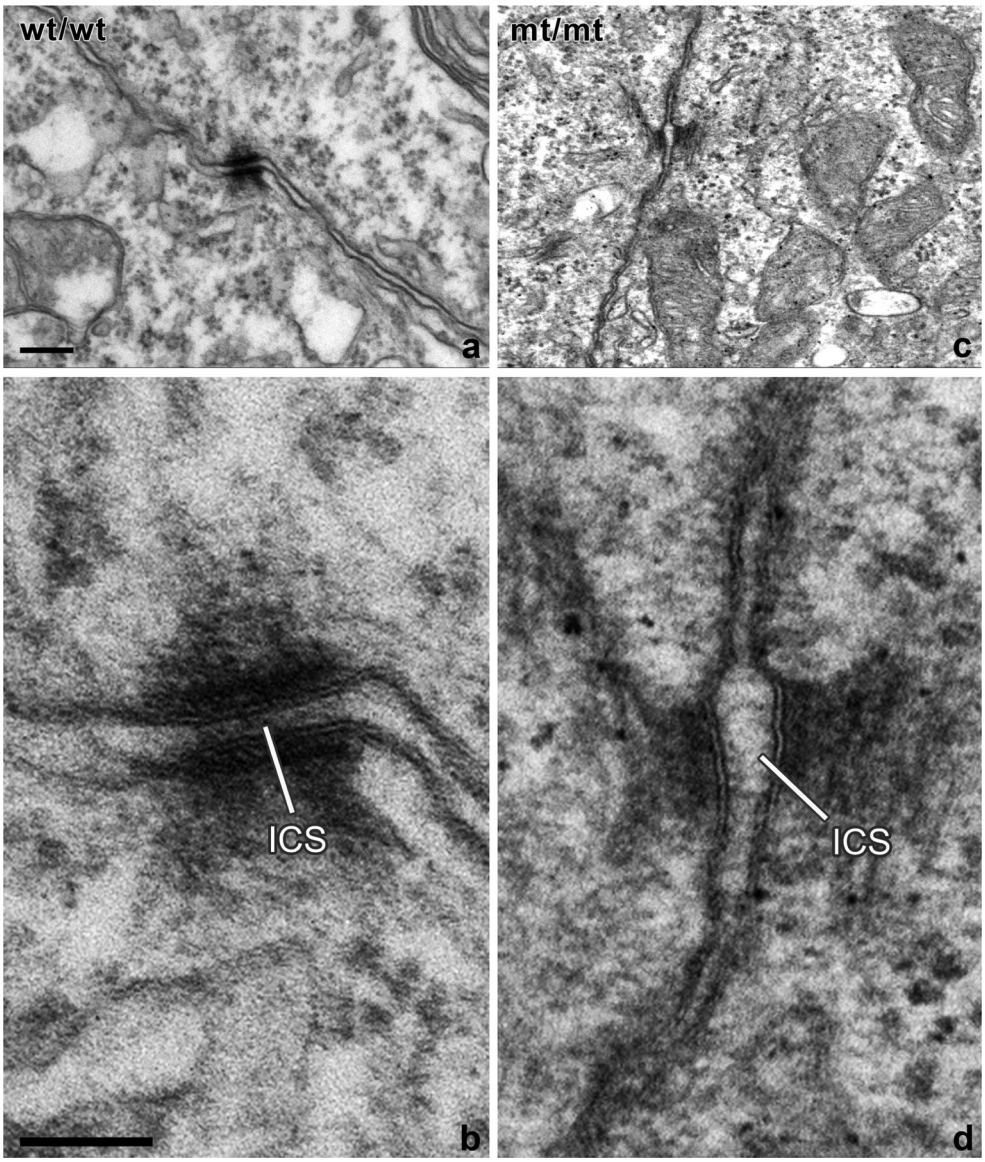

Fig. 5 Comparison of desmosomal intercellular spaces (ICS) in endometrial epithelium of wild type (wt/wt; **a**, **b**) and mutant mice (mt/mt; **c**, **d**). In wild type animals, the intercellular space of desmosomes shows an electron-dense structure (**b**), which cannot be identified in desmosomes of mutant animals (**d**). Scale bars 200 nm

93.51 ± 1.79 nm for the wild type and 95.18 ± 1.83, $p = 0.52$, for the mutant.

Grey scale analysis with the line profile analysis tool of Image-Pro Plus 5.0.

To confirm the linear measurement data, measurements were performed with an additional method using grey scale analysis. Out of 100 desmosomes for each genotype, which was blinded for the observer, 61 desmosomes were evaluated for the wild type and 71 desmosomes for the mutant. The intercellular space and the widths of the outer dense plaques were evaluated.

The mean ± SEM of the intercellular space was 15.76 ± 0.31 nm for the wild type and 18.65 ± 0.47 nm for the mutant (Fig. 7). The means of the measured width of the intercellular space were again significantly different: $p < 0.0001$.

In contrast, the means of the measured width of the two outer dense plaques did not differ between wild type and mutant. The mean ± SEM of the width of the ODP was 16.46 ± 0.23 nm for the wild type and 16.46 ± 0.24 nm for the mutant, $p = 0.99$.

Discussion

This is the first study to investigate the influence of Dsg2 mutation on the structure and number of desmosomes in the simple epithelium of the mouse uterine endometrium. Ultrastructural and immunohistochemical analysis was performed, and the analysed data were statistically

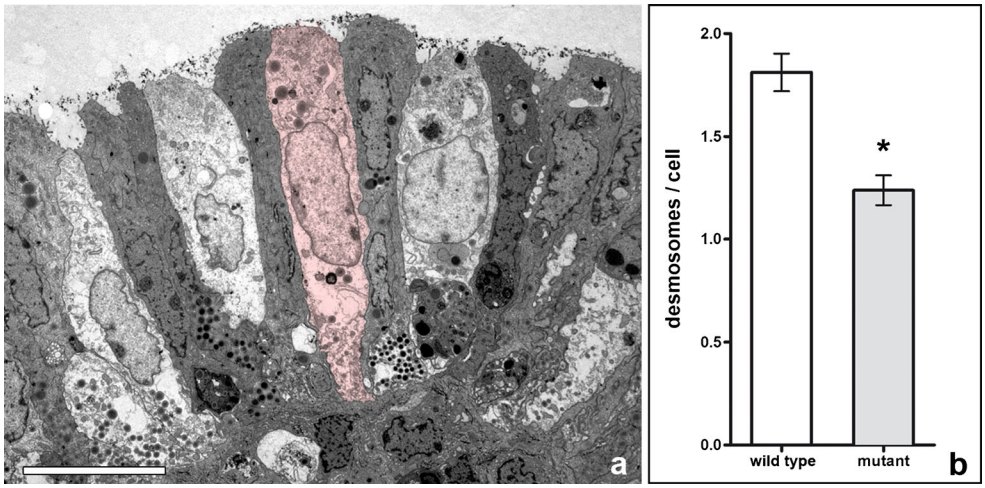

Fig. 6 **a** Electron microscopy of endometrial epithelium showing a typical longitudinal section of an epithelial cell (coloured), which was evaluated for desmosomes at the lateral cell membranes according to the criteria mentioned above. Scale bar 10 μm. **b** Each cell analysed was one cell distant from the next evaluated cell. The desmosomes at the lateral membranes per cell were counted. The mean value for the number of desmosomes per cell was 1.81 ± 0.09 for the wild type and 1.24 ± 0.07 for the mutant animals. The difference between the two groups was significant: $*p < 0.0001$

evaluated. The ultrastructural measurements included the width and length of the two outer dense plaques and the width of the intercellular desmosomal space. The distribution and intensity of the desmosomal plaque protein desmoplakin and the mutant cadherin desmoglein 2 were detected by immunofluorescence.

Dsg2 immunofluorescence was strongly reduced in the luminal and glandular uterine epithelium of homozygous mice lacking parts of the extracellular EC1/EC2 domains of the Dsg2 protein but Dsp immunofluorescence was also diminished indicating a reduced number of desmosomes. Morphometric analysis at the ultrastructural level also revealed a reduction of desmosomes per cell, i.e., to 68% compared to the wild type. By means of further electron microscopy evaluation, the length and width of the outer dense plaques were measured. These plaques did not differ from the desmosomal plaques of the wild type indicating that this mutation of Dsg2 does not interfere with plaque formation (Fujiwara et al. 2015; Lowndes et al. 2014).

By measuring the intercellular desmosomal space, a significantly wider extracellular gap was detected in the mutant mice. This is in accordance with the findings of Kant et al. (2012), who observed a widening of the intercellular space in intercalated discs of Dsg2-mutant hearts. Studies on endomyocardial biopsies of patients with arrhythmogenic right ventricular cardiomyopathy (ARVC) (Basso et al. 2006; Pilichou et al. 2006) also revealed a decreased number of desmosomes and widening of the intercellular desmosomal gap.

One of the first descriptions of the dimensions of the intercellular space was given by Farquhar and Palade (Farquhar and Palade 1963), who determined its size to be about 24 nm. The references to the calculated distances vary according to the different methods of embedding and treating the tissues as well as between the different tissue specimens. This variability may be caused by different degrees of fixation-induced tissue shrinkage (North et al. 1999). The lowest values for the intercellular space range from 15 to 25 nm for conventional transmission electron microscopy to 35 ± 3 nm (Al-Amoudi et al. 2007) for cryoelectron microscopy of vitreous sections.

In our study, the mean value for the intercellular space obtained by linear measurement was about 15 nm for the wild type and about 19 nm for the mutant. In addition, measurements were confirmed by grey scale analysis and performed blinded to avoid any bias.

The main result of the ultrastructural analysis in our study was the significant difference between the width of the intercellular space of wild type and mutant.

In the Dsg2 mutant mouse, exons 4–6 are lacking and exon 3 is spliced in frame to exon 7 (Krusche et al. 2011). Therefore, important domains that are known to participate in cis- and trans-interaction, notably, the main *N*-glycosylation site and one of the calcium-binding domains are missing. We therefore propose that the mutated Dsg2 is less adhesive.

Though the cadherin-specific conserved amino acid tryptophan2, which has a special function in the trans-interaction of cadherin-domains adhering at the hydrophobic region, was not deleted, all amino acids that code for the hydrophobic binding are lacking.

In addition, also the amino acids that are responsible for the cis-interaction of the cadherin domains (Boggon

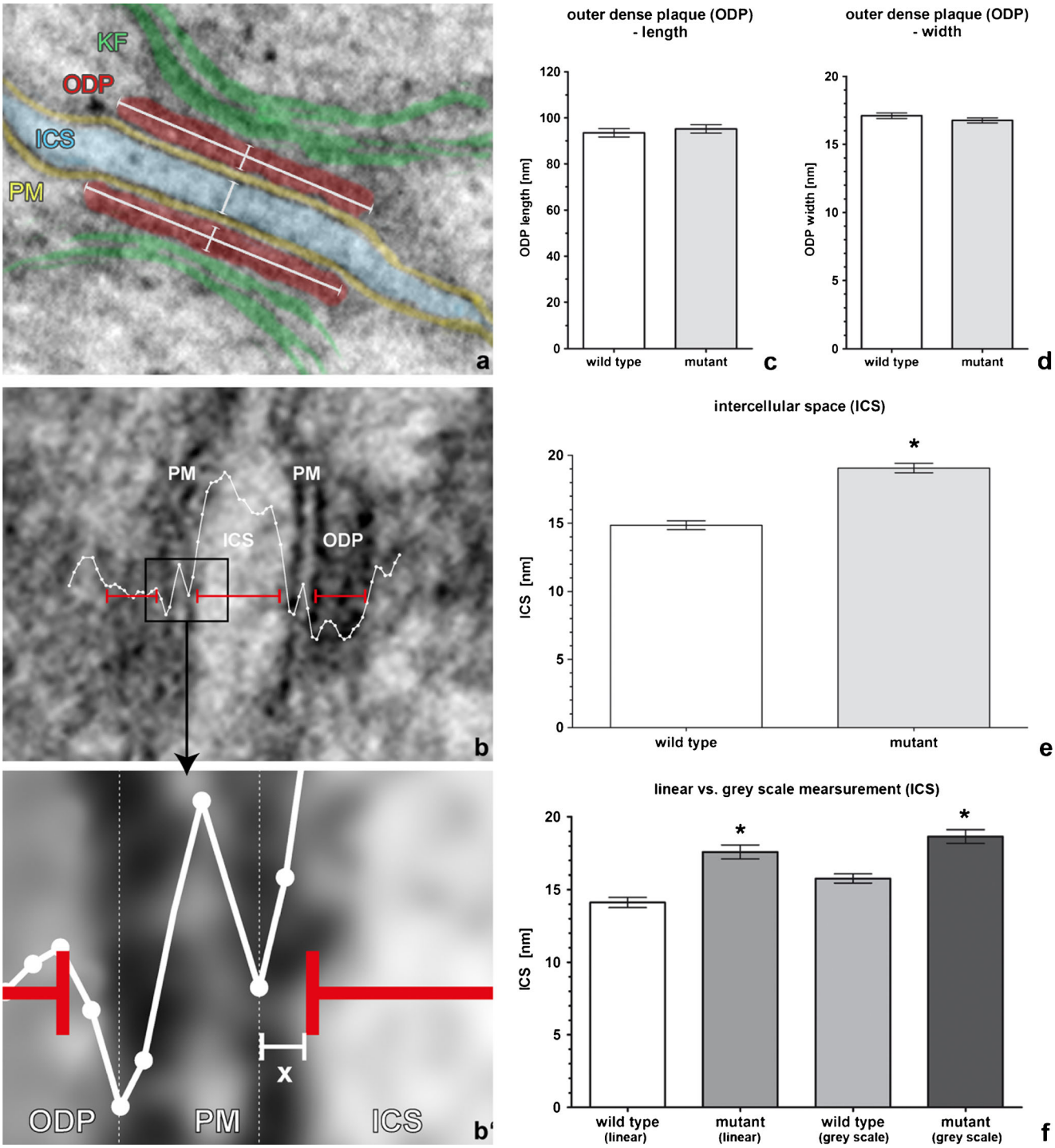

Fig. 7 Linear measurement and grey scale analysis. **a** Electron microscopy of a typical desmosome with coloured structures: Green: KF keratin filaments; red: ODP outer dense plaques; yellow: PM plasma membranes; blue: ICS intercellular space. Measurements of the length and width of the outer dense plaques and the intercellular space are indicated by white lines. **b** Comparison of linear measurement vs grey scale analysis. The red lines indicate the measured dimensions. The graph (white line) indicates the intensity plot of the grey scale analysis. **b′** Schematic depicting the differences in measurements due to the composition of the lipid bilayer. In the linear measurement, the intercellular space is measured between the outer margins of the two adjacent plasma membranes. In the grey scale analysis, the intercellular space is measured between the relative minima in intensity (darker areas) of the outer leaflets of the lipid bilayers of adjacent cells. Therefore, the measurement of the grey scale analyses leads to a higher value (+ x) for the intercellular space compared to linear measurement. **c**, **d** Mean length ± SEM (**c**) and mean width ± SEM (**d**) of the outer dense plaques (ODP) showed no significant difference between the wild type and mutant animals. **e** Mean ± SEM of the desmosomal intercellular space (ICS) for the wild type and the mutant. The difference is significant: $*p < 0.0001$. **f** Mean ± SEM of the desmosomal intercellular space (ICS) evaluated by the two different measurements, the linear measurement and the grey scale measurement. The difference obtained by each method differs significantly ($*p < 0.0001$) between the wild type and mutant

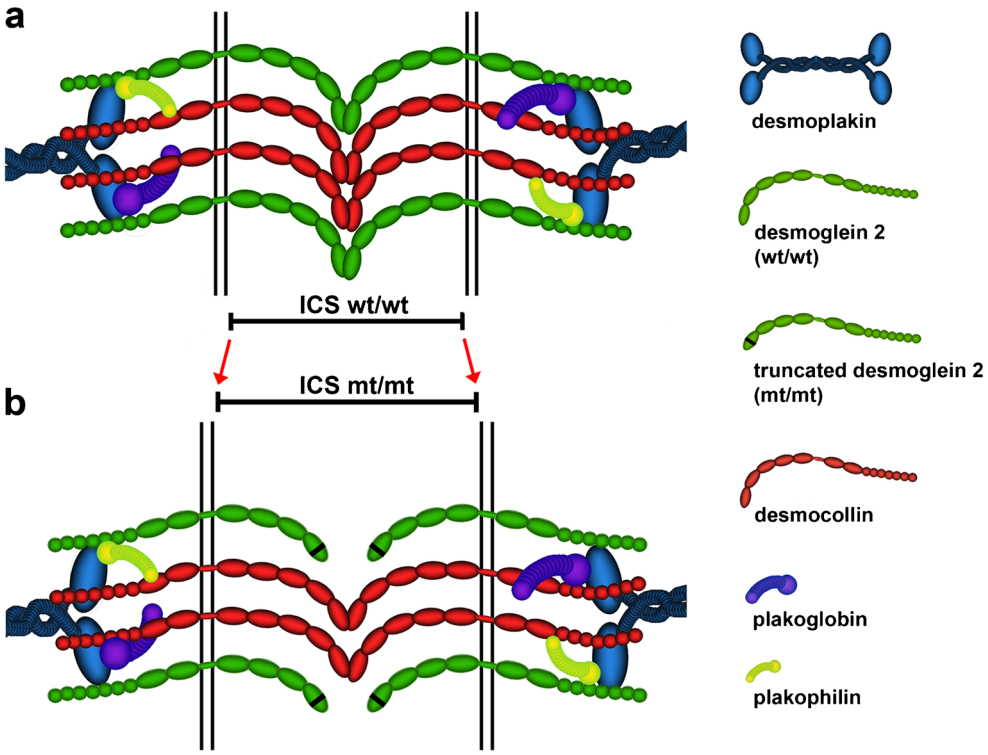

Fig. 8 Model showing interaction between desmosomal cadherins. **a** Interaction of the cadherins Dsg2 und Dsc2 in the desmosomal intercellular space; ICS wt/wt = width of the intercellular space in the wild type. **b** Proposed change of the interaction of the cadherins Dsg2 and Dsc2 in the desmosomal intercellular space in the mutant mouse lacking major parts of the extracellular EC1-EC2 domains resulting in reduced cis-trans-interaction, extension of the trans-dimers and finally in widening of the intercellular space; ICS mt/mt = width of the intercellular space in the mutant

et al. 2002) are missing in the mutated Dsg2 (Holthofer 2007).

The deleted parts of Dsg2 are important for adhesion through homo- and heterophilic desmosomal cadherin interactions. The partial loss of extracellular domains of Dsg2 probably results in reduced overlap of homophilic cis- and trans-interactions as well as heterophilic interactions with desmocollin 2 leading to a widened intercellular space with reduced cellular adhesion as illustrated schematically in Fig. 8.

Furthermore, in the Dsg2 mutant mouse, which lacks substantial parts of the extracellular EC1–EC2 domains of the desmosomal cadherin, no electron-dense midline could be detected, whereas in wild type animals, the intercellular space of desmosomes shows an electron-dense structure.

In a previous study by our group, we showed that the density and distribution of desmosomes in human uterine epithelium are hormonally regulated during the menstrual cycle (Buck et al. 2012). In addition, a functional correlation between desmosomes and embryo implantation has been deduced from animal studies (Illingworth et al. 2000; Preston et al. 2004, 2006) and from cell culture experiments using human cells (Buck et al. 2015).

In the present work, we showed that truncation of the desmosomal cadherin desmoglein 2 led to a visible change on the ultrastructural level and to a significant reduction in desmosomes per cell. These results might explain to some extent the reduced fertility of homozygous $Dsg2^{mt/mt}$ mice, which remains to be further investigated.

Compliance with ethical standards

Ethical approval All procedures performed in studies involving animals were in accordance with the ethical standards of the institution or practice at which the studies were conducted. This article does not contain any studies with human participants performed by any of the authors.

References

Al-Amoudi A, Frangakis AS (2008) Structural studies on desmosomes. Biochem Soc Trans 36:181–187

Al-Amoudi A, Diez DC, Betts MJ, Frangakis AS (2007) The molecular architecture of cadherins in native epidermal desmosomes. Nature 450:832–837

Basso C, Czarnowska E, Della Barbera M, Bauce B, Beffagna G, Wlodarska EK, Pilichou K, Ramondo A, Lorenzon A, Wozniek O, Corrado D, Daliento L, Danieli GA, Valente M, Nava A, Thiene G, Rampazzo A (2006) Ultrastructural evidence of intercalated disc remodelling in arrhythmogenic right ventricular cardiomyopathy: an electron microscopy investigation on endomyocardial biopsies. Eur Heart J 27:1847–1854

Boggon TJ, Murray J, Chappuis-Flament S, Wong E, Gumbiner BM, Shapiro L (2002) C-cadherin ectodomain structure and implications for cell adhesion mechanisms. Science 296:1308–1313

Broussard JA, Getsios S, Green KJ (2015) Desmosome regulation and signaling in disease. Cell Tissue Res 360:501–512

Buck VU, Windoffer R, Leube RE, Classen-Linke I (2012) Redistribution of adhering junctions in human endometrial epithelial cells during the implantation window of the menstrual cycle. Histochem Cell Biol 137:777–790

Buck VU, Gellersen B, Leube RE, Classen-Linke I (2015) Interaction of human trophoblast cells with gland-like endometrial spheroids: a model system for trophoblast invasion. Hum Reprod 30:906–916

Byers SL, Wiles MV, Dunn SL, Taft RA (2012) Mouse estrous cycle identification tool and images. PLoS One 7:e35538

Eshkind L, Tian Q, Schmidt A, Franke WW, Windoffer R, Leube RE (2002) Loss of desmoglein 2 suggests essential functions for early embryonic development and proliferation of embryonal stem cells. Eur J Cell Biol 81:592–598

Farquhar MG, Palade GE (1963) Junctional complexes in various epithelia. J Cell Biol 17:375–412

Fujiwara M, Nagatomo A, Tsuda M, Obata S, Sakuma T, Yamamoto T, Suzuki ST (2015) Desmocollin-2 alone forms functional desmosomal plaques, with the plaque formation requiring the juxtamembrane region and plakophilins. J Biochem 158:339–353

Garrod D, Chidgey M (2008) Desmosome structure, composition and function. Biochim Biophys Acta 1778:572–587

Holthofer B (2007) Konditionale Mutagenese von Desmoglein 2 in der Maus. Institute of Anatomy, Johannes Gutenberg-University, Mainz. Dissertation, pp 1–208. https://publications.ub.uni-mainz.de/theses/frontdoor.php?source_opus=1540

Holthofer B, Windoffer R, Troyanovsky S, Leube RE (2007) Structure and function of desmosomes. Int Rev Cytol 264:65–163

Illingworth IM, Kiszka I, Bagley S, Ireland GW, Garrod DR, Kimber SJ (2000) Desmosomes are reduced in the mouse uterine luminal epithelium during the preimplantation period of pregnancy: a mechanism for facilitation of implantation. Biol Reprod 63:1764–1773

Kamekura R, Kolegraff KN, Nava P, Hilgarth RS, Feng M, Parkos CA, Nusrat A (2014) Loss of the desmosomal cadherin desmoglein-2 suppresses colon cancer cell proliferation through EGFR signaling. Oncogene 33:4531–4536

Kant S, Krull P, Eisner S, Leube RE, Krusche CA (2012) Histological and ultrastructural abnormalities in murine desmoglein 2-mutant hearts. Cell Tissue Res 348:249–259

Koch PJ, Walsh MJ, Schmelz M, Goldschmidt MD, Zimbelmann R, Franke WW (1990) Identification of desmoglein, a constitutive desmosomal glycoprotein, as a member of the cadherin family of cell adhesion molecules. Eur J Cell Biol 53:1–12

Koch PJ, Goldschmidt MD, Walsh MJ, Zimbelmann R, Franke WW (1991) Complete amino acid sequence of the epidermal desmoglein precursor polypeptide and identification of a second type of desmoglein gene. Eur J Cell Biol 55:200–208

Kowalczyk AP, Green KJ (2013) Structure, function, and regulation of desmosomes. Prog Mol Biol Transl Sci 116:95–118

Krusche CA, Holthofer B, Hofe V, van de Sandt AM, Eshkind L, Bockamp E, Merx MW, Kant S, Windoffer R, Leube RE (2011) Desmoglein 2 mutant mice develop cardiac fibrosis and dilation. Basic Res Cardiol 106:617–633

Lowndes M, Rakshit S, Shafraz O, Borghi N, Harmon RM, Green KJ, Sivasankar S, Nelson WJ (2014) Different roles of cadherins in the assembly and structural integrity of the desmosome complex. J Cell Sci 127:2339–2350

McDowell EM, Trump BF (1976) Histologic fixatives suitable for diagnostic light and electron microscopy. Arch Pathol Lab Med 100:405–414

Nava P, Laukoetter MG, Hopkins AM, Laur O, Gerner-Smidt K, Green KJ, Parkos CA, Nusrat A (2007) Desmoglein-2: a novel regulator of apoptosis in the intestinal epithelium. Mol Biol Cell 18:4565–4578

North AJ, Bardsley WG, Hyam J, Bornslaeger EA, Cordingley HC, Trinnaman B, Hatzfeld M, Green KJ, Magee AI, Garrod DR (1999) Molecular map of the desmosomal plaque. J Cell Sci 112(Pt 23):4325–4336

Pilichou K, Nava A, Basso C, Beffagna G, Bauce B, Lorenzon A, Frigo G, Vettori A, Valente M, Towbin J, Thiene G, Danieli GA, Rampazzo A (2006) Mutations in desmoglein-2 gene are associated with arrhythmogenic right ventricular cardiomyopathy. Circulation 113:1171–1179

Preston AM, Lindsay LA, Murphy CR (2004) Progesterone treatment and the progress of early pregnancy reduce desmoglein 1&2 staining along the lateral plasma membrane in rat uterine epithelial cells. Acta Histochem 106:345–351

Preston AM, Lindsay LA, Murphy CR (2006) Desmosomes in uterine epithelial cells decrease at the time of implantation: an ultrastructural and morphometric study. J Morphol 267:103–108

Reynolds ES (1963) The use of lead citrate at high pH as an electron-opaque stain in electron microscopy. J Cell Biol 17:208–212

Rugh R (1968) The mouse; its reproduction and development. Oxford University Press, New York

Schafer S, Koch PJ, Franke WW (1994) Identification of the ubiquitous human desmoglein, Dsg2, and the expression catalogue of the desmoglein subfamily of desmosomal cadherins. Exp Cell Res 211:391–399

Schafer S, Stumpp S, Franke WW (1996) Immunological identification and characterization of the desmosomal cadherin Dsg2 in coupled and uncoupled epithelial cells and in human tissues. Differentiation 60:99–108

Schlegel N, Meir M, Heupel WM, Holthofer B, Leube RE, Waschke J (2010) Desmoglein 2-mediated adhesion is required for intestinal epithelial barrier integrity. Am J Physiol Gastrointest Liver Physiol 298:G774–G783

Spindler V, Meir M, Vigh B, Flemming S, Hutz K, Germer CT, Waschke J, Schlegel N (2015) Loss of Desmoglein 2 contributes to the pathogenesis of Crohn's disease. Inflamm Bowel Dis 21:2349–2359

Thomason HA, Scothern A, McHarg S, Garrod DR (2010) Desmosomes: adhesive strength and signalling in health and disease. Biochem J 429:419–433